ACS OMEGA

http://pubs.acs.org/journal/acsodf

Article

Synthesis, Characterization, Computational Studies, Molecular Docking, and *In Vitro* Anticancer Activity of Dihydropyrano[3,2-*c*]chromene and 2-Aminobenzochromene Derivatives

Surya Cholayil Palapetta, Harichandran Gurusamy,* and Sudhandiran Ganapasam

Cite This: *ACS Omega* 2023, 8, 7415−7429

Read Online

ACCESS | Metrics & More | Article Recommendations | Supporting Information

ABSTRACT: 2-Aminobenzochromenes and dihydropyranochromenes represent a unique class of biologically active compounds. Recent organic syntheses focus on the development of environmentally benign synthetic protocols, and as a part of this concept, we have taken a considerable interest in the synthesis of this class of biologically active compounds using an environment-friendly, reusable heterogeneous Amberlite IRA 400-Cl resin catalyst. This work further aims to highlight the importance and advantages of these compounds and to compare the experimental data obtained with those of the theoretical calculations made using the density functional theory (DFT) method. Molecular docking studies on the selected compounds were also carried out to study the effectiveness of these compounds in liver fibrosis treatment. Furthermore, we have performed molecular docking studies and an *in vitro* study of the anticancer activity of dihydropyrano[3,2-*c*]chromenes and 2-aminobenzochromenes against human colon cancer cells [HT29].

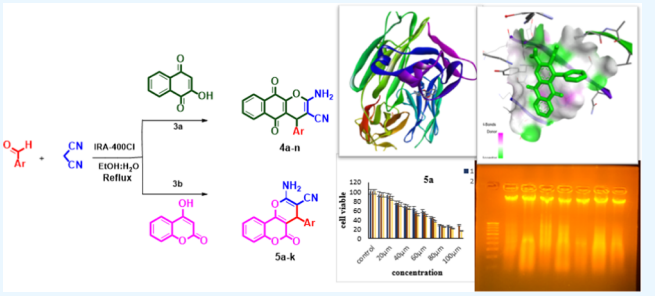

1. INTRODUCTION

Chromenes together with the benzochromene nucleus have emerged as a promising and attractive scaffold due to their biological applications in different subjects.[1] This class of compounds together demonstrates unbelievable applications in antibacterial,[2] anticancer,[3] antileishmanial,[4] antioxidant,[5] vascular-disrupting,[6] blood platelet antiaggregating analgesic,[7] and hypolipidemic effects[8] along with antineurodegenerative disorders such as Alzheimer's and Parkinson disease[9−11] and many more. Among the functionalized chromenes, dihydropyrano[3,2-*c*]chromenes and aminobenzochromenes are in particular the heterocyclic scaffolds that are biologically significant and hence medicinally privileged.

In addition to biological activity, some chromenes also exhibit photophysical properties. The varied applications of chromenes, especially dihydropyrano[3,2-*c*]chromenes and aminobenzochromenes, have prompted many researchers to pay attention to the synthesis of this group of compounds.

A literature survey reveals that there are a few methods known for the synthesis of dihydropyrano[3,2-*c*]chromenes and 2-aminobenzochromenes from aromatic aldehyde 2-hydroxy-1,4-naphthaquinone/4-hydroxycoumarin using various catalysts such as DBU,[12] L-proline as a basic organocatalyst,[13] a catalytic amount of Et_3N in CH_3CN,[14] triethylammonium hydrogen sulfate ($[Et_3NH][HSO_4]$) as a Brønsted acidic ionic liquid,[15] *o*-benzenedisulfonamide (OBS), enzyme Lipase,[16] silica-supported boron trifluoride (BF_3·SiO_2),[17] ZIF@$ZnTiO_3$ nanocomposite,[18] cobalt-doped iron(III) tartrate complex[19] catalyzed under microwave irradiation in water, heterogeneous sulfonic acid-functionalized silica (SiO_2-Pr-SO_3H) solid acid catalyst,[20] and thiourea dioxide catalyst.[21]

Even though several reports are known for the synthesis of dihydropyrano[3,2-*c*]chromenes and 2-aminobenzochromenes, to the best of our knowledge, MCR synthesis using heterogeneous Amberlite 400-Cl resin as a catalyst is not known. Thus, here, we wish to report a multicomponent synthesis of dihydropyrano[3,2-*c*]chromenes and amino benzo[*g*]chromenes using Amberlite 400-Cl resin as a catalyst in the presence of 1:1 EtOH/H_2O as a solvent under reflux conditions.

In the recent past, ion-exchange resins were used as a catalyst in various organic transformations such as Knoevenagel, Michael[22] condensations, the preparation of heterocyclic ketols,[23] the synthesis of nitriles,[24] C-acylation of phenols,[25]

Received: September 19, 2022
Accepted: January 25, 2023
Published: February 17, 2023

decarboxylation,[26] and amide formation and have gained considerable importance due to their nontoxicity, low cost, and high yield efficiency. The main success of this resin as a catalyst is that it can be regenerated and reused. Also, the catalyst resin used here has the added advantage of short reaction time and easy simple isolation of the products; this helps us to carry out an environment-friendly procedure with excellent yields.

Chemotherapy is one of the potential treatments for prolonging the patient's life. As a part of our ongoing research progressions, we have explored the biological aspect of these compounds. Cell viability assay has been gaining much attention as an alternative to using animals. It is useful, for example, in screening a large number of chemicals for their cytotoxicity to various cells. The 3-[4,5-dimethylthiazol-2-yl]-2,5-diphenyltetrazolium bromide (MTT) assay is a sensitive, quantitative, and reliable colorimetric assay that measures the viability, proliferation, and activation of cells and used to study the inhibitory potential with IC50 values.[27,28] Apart from this, theoretical calculations based on the properties of some selected derivatives have also been performed using the density functional theory (DFT) method.

2. MATERIALS AND METHODS

2.1. Materials. All of the aldehydes, malononitrile, and C−H-activated compounds were purchased from Sigma Aldrich (USA), Spectrochem (India), and SRL (India) and were used without further purification. All solvents were kept sealed in airtight bottles as well to minimize the absorption of atmospheric moisture. Moreover, they were distilled before being used. The products were characterized by their physical constants, comparison with authentic samples, and IR (Thermo Mattson Satellite FT-IR spectrophotometer) and NMR spectroscopies with a Bruker UltraShield spectrometer (400 and 100 MHz) in the DMSO-d_6 solvent using tetramethylsilane (TMS) as an internal standard. Melting points were measured using an electrothermal melting point apparatus in capillary tubes. Mass spectra were measured on a Waters$^{(R)}$ Micromass$^{(R)}$Q-TOF micromass spectrometer. Light microscopy (Motic, Hongkong) was used to visualize the cells.

2.2. General Procedure for the Synthesis of 2-Amino-4*H*-benzo[*g*]chromenes and Dihydropyrano[3,2-*c*]-chromene Derivatives. In a 50 mL round-bottom flask, a mixture of aromatic aldehydes **1(a−n)** (1 mM), malononitrile **2** (1.5 mM), and 2-hydroxy-1,4-naphthaquinone **3a**/4-hydroxycoumarin **3b** (1 mM) were mixed in EtOH/H_2O (1:1) solvent in the presence of Amberlite IRA-400-Cl resin as a catalyst, the reaction mixture was stirred at 80° C, and the time duration is mentioned in Table 2. The progress of the reaction was monitored by thin-layer chromatography (TLC). Later, on completion of the reaction as directed by TLC, the reaction mixture was cooled to a suitable temperature to get the precipitate. The precipitate thus obtained was dissolved in ethyl acetate, and the catalyst was filtered off, and the solvent was removed using a rotavaporator. The crude solid precipitate was purified by recrystallization from ethanol to get the corresponding pure products. The products were characterized by Fourier transform infrared spectroscopy (FT-IR), ^{1}H NMR, and ^{13}C NMR, and their physical constants were compared with those of the reported samples.

2.3. Anticancer Activity of Dihydropyrano[3,2-*c*]-chromenes and 2-Aminobenzochromenes against Colon Cancer Cells [HT29 Cell Line]. Cancer has become the most dreadful disease; it appears to be a major cause of morbidity and mortality. The World Health Organization (WHO) has recorded cancer as one of the leading causes of death in the world. Therefore, developing new anticancer drugs with fewer side effects is an important task in this field. It is estimated that a lot of effort, money, and time are associated with the successful approval of a single drug due to the fast development and lifestyle and the urgent need for drug screening and toxicity analysis. Cell viability is an important technique in cancer chemotherapy since it is useful in screening a large number of chemicals for their cytotoxicity to various cells. The cell viability technique screens a large number of compounds synthesized toward various cells and thus becomes an alternative to animal experiments and has been gaining attention in new drug development. The molecules comprising a 2*H*/4*H*-chromene scaffold show beneficial effects, such as anticancer, antidiabetic and antimicrobial properties.[29,30]

2.3.1. Cell Culture. HT29 cells were procured from the National Centre for cell science, Pune, India, and grown in DMEM medium (Hi-media, India) supplemented with 4.5 g of glucose per liter, L-glutamine, 3.7 g per liter of sodium bicarbonate, and 1 mM sodium pyruvate supplemented with 10% heat-inactivated fetal bovine serum (FBS) 100 U/mL penicillin and 100 μg/mL streptomycin at 37 °C under a humidified atmosphere of 5% CO and 95% air. For periodical maintenance of cells, 1×10^7 cells were routinely maintained in culture and experimental vessels.

2.3.2. 3-[4,5-Dimethylthiazol-2-yl]-2,5-diphenyl-tetrazolium Bromide (MTT) Assay. The MTT colorimetric assay was conducted on 96-well cell culture plates (Tarsons, India). After the cells attained confluence, 5×10^3 cells in serum-free medium were seeded in 96-well plates and incubated for 24 h. The synthesized compounds (**4j**, **4m**, **4n**) (**5a**, **5g**, **5j**, **5k**) were added and incubated at different times and doses in a dependent manner. After 0−48 h of incubation, 50 μL of MTT reagent (Abcam) was added and incubated in the dark for up to 4 h, and the medium was discarded. Next, 100 μL of dimethyl sulfoxide (DMSO) solvent was added, wrapped in foil, and shaken for 5 min, and absorbance was read at 590 nm in an ELISA plate reader.[31,32] Graphs were plotted, and the IC_{50} value was determined for the cytotoxicity of the synthesized compounds.

2.3.3. Light Microscopy. HT29 cells were seeded in 24-well plates and treated with chromenes for definite time points. After the cellular treatments with chromenes, the cells were visualized in inverted light microscopy (Motic, Hongkong) using a 20× objective, and the morphological changes were captured.

2.3.4. DNA Fragmentation Analysis. HT 29 cells were seeded in a 6-well plate and incubated at 37 °C with 5% CO_2. After attaining 60% confluency, the cells were treated with the synthesis compounds. DNA was isolated from the control, and the cells were treated using a DNA extraction kit and using phenol:chloroform:isoamyl alcohol. The extracted DNA was precipitated using phenol, chloroform, and isoamyl alcohol overnight, and DNA was quantified and stored at −20 °C until analysis. The isolated DNA and 100 kb DNA ladder were run in a 1.5% agarose gel electrophoresis using 50 V. The DNA was visualized when stained with the ethidium bromide dye in the dark for 10 min with destaining with water.

https://doi.org/10.1021/acsomega.2c06049
ACS Omega 2023, 8, 7415−7429

Table 1. Optimization Reaction for the Synthesis of Compounds 4 and 5

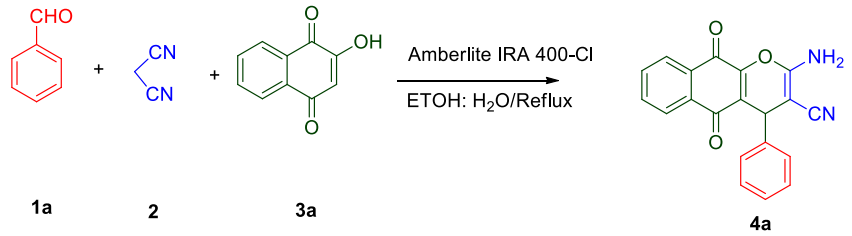

1a 2 3a 4a

entry	catalyst (% mmol)	temp. (°C)	time (h)	product yield (%)
1	Nil	25	8	
2	Nil	80	8	trace
3	NaCl	25	8	
4	KCl	25	8	trace
5	NH_4Cl	25	8	trace
6	*n*-Bu_4NCl	25	8	trace
7	$BnMe_3NCl$		8	trace
4	AER (**200/0.6**)	**80**	**3**	**95**
5	AER (300/0.9)	80	3	95
6	AER (500/1.5)	80	3	95
7	AER (100/0.3)	80	3	60
8	CER (200/0.6)	80	3	90

3. RESULTS AND DISCUSSION

To optimize the reaction for the synthesis of 2-amino-4*H*-benzo[*g*]chromene derivatives in a well-organized way, the reaction of benzaldehyde (1 equiv), malononitrile (1.2 equiv), and 2-hydroxy-1,4-naphthoquinone (1 equiv) was selected as a model reaction. When the reaction was carried out in the absence of a catalyst, no product formation was observed (Table 1, entry 1). Also, when the reaction mixture was heated to 80 °C in the absence of a catalyst, there was not much considerable product formation observed (Table 1, entry 2). The result was the same when the reaction was repeated with an ionic catalyst (Table 1 entries 3, 4, 5, 6, 7). A remarkable product conversion was observed when the reaction mixture was refluxed for 3 h at 80 °C in the presence of Amberlite IRA 400-Cl resin, a solid heterogeneous catalyst (Table 1, entry 4). When the catalyst loading was increased, there was no change in the product yield (Table 1, entries 5, 6). When the catalyst loading was decreased, the product conversion was reduced to 60%. (Table 1, entry 7). The reaction also worked well with cation exchange resin to give a product yield of 90% (Table 1, entry 8).

The competence of the model reaction conditions was later investigated with diversely substituted aromatic and hetero-aromatic aldehydes (**1a-n**), with malononitrile **2** and 2-hydroxy-1,4-naphthaquinone **3a** in 1:1 ethanol:water under reflux conditions. The results obtained are summarized in Table 2. The different aromatic aldehydes tried gave considerably good yields irrespective of the electron-withdrawing or electron-donating nature. This illustrates that the substituents on aldehydes have nothing to do with the yield of the reaction.

All the synthesized compounds were characterized with various spectroscopic techniques such as ^{1}H NMR, ^{13}C NMR, and FT-IR, and selected compounds were confirmed with HRMS also. Inspired by these results, we attempted to extend the same protocol of synthesis to another set of reactions, where 2-hydroxy-1,4-naphthaquinone was replaced with 4-hydroxycoumarin to produce dihydropyrano[3,2-*c*]chromenes. The reaction was carried out with different aromatic aldehyde (**1a−k**), and the structures of the various compounds are shown in Table 3.

All the synthesized compounds were characterized and confirmed by various spectroscopic studies such as ^{1}H NMR, ^{13}C NMR, and FT-IR and selected compounds were characterized with HRMS also.

3.1. Significance of the Catalyst. To realize the important ability of reusability of the catalyst, we tried to reuse the catalyst recovered from the reaction. After the complete conversion of the reaction, the catalyst was recovered by filtration, washing with ethanol, and drying and then reused for the next reaction. The recovered catalyst was able to carry out the reaction to produce the expected product in 96% yield. The catalyst was recovered and reused five times on average without loss of its activity, which shows the practical reuse and recycling ability of this catalyst (Figure 1).

3.2. Plausible Mechanism for the Formation of Compounds 4 and 5. Based on the above-mentioned protocol, we hereby propose an Amberlite IRA-400-Cl resin catalyst-aided mechanism for the synthesis of compound **4**/**5** (Scheme 1). Amberlite resin ionizes in the presence of the solvent to form OH and HCl. The reaction is supposed to proceed through the formation of a Knoevenagel intermediate (A) and is then attacked by the enolate of the C−H-activated compound (**3a**, **3b**), giving rise to an adduct (B), which eventually undergoes ring closure to afford the desired product **4**/**5**.

3.3. Computational Details. Theoretical calculations have been performed for the selected compounds by DFT using the Gaussian 09 program[35,36] and visualized in GaussView. The optimized structural parameters obtained using B3LYP/6-311G(d,p) have been evaluated for the calculation of various parameters such as vibrational frequencies with FMO analysis including the calculation of orbital energies, electron affinity, and electrophilicity index. The molecular electrostatic potential surfaces (MEPs) were visualized using GaussView.

3.4. Molecular Geometry. The optimized structure of the compounds was calculated using the B3LYP 6-311G(d,p)

https://doi.org/10.1021/acsomega.2c06049
ACS Omega 2023, 8, 7415−7429

Table 2. Synthesis of 2-Amino-4*H*-benzo[*g*]chromenes Derivatives

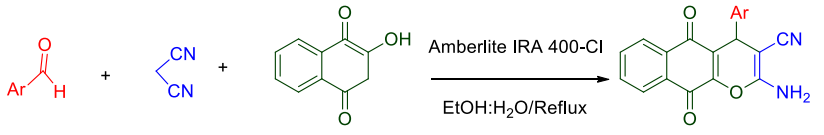

1a-n 2 3a 4a-n

Entry	Aldehyde (1 mM)	Time (hr)	1,3-Diketone	Product/ [yield%]	m. pt. ^{0}C	References
1	Benzaldehyde 1a	2	3a	4a [98]	256-260	260-263 [15]
2	4-Nitrobenzaldehyde1b	2	3a	4b [95]	228-230	192-196 [33]
3	3-Nitrobenzaldehyde 1c	3	3a	4c [93]	246-247	248-249[33]
4	4-Cyanobenzaldehyde 1d	2	3a	4d [92]	240-242	198-200[33]
5	4-Chlorobenzaldehyde 1e	3	3a	4e [93]	245-247	250-251[15]
6	4-Fluorobenzaldehyde 1f	3	3a	4f [92]	255-266	285-287 [15]
7	4-Methylbenzaldehyde 1g	3	3a	4g [93]	240-242	240-242[15]
8	4-Methoxybenzaldehyde 1h	3	3a	4h [90]	248-250	246-248 [15]
9	2-Hydroxy benzaldehyde 1i	2	3a	4i [92]	234-240	----------[15]
10	Thiophene 2- aldehyde 1j	3	3a	4j [93]	224-226	----------[15]
11	4-Pyridinecarboxaldehyde 1k	3	3a	4k [90]	264-268	272–274 [33]
12	3-Pyridinecarboxaldehyde 1l	3	3a	4l [88]	268-270	This work
13	Indole-3-carboxaldehyde 1m	3	3a	4m [91]	206-210	This work
14	Terephthaldehyde 1n	3	3a	4n [90]	254-260	This work

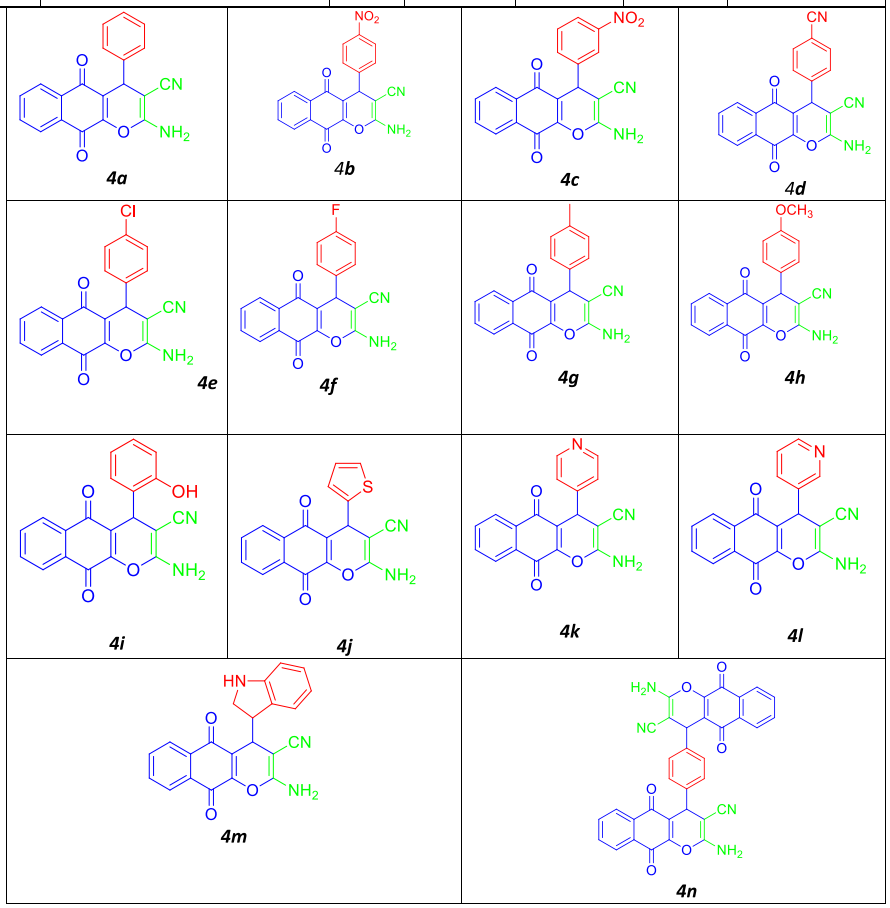

method and was viewed using the Chemcraft program and is shown in Figure 2.

3.5. Infrared Spectra. The experimental and theoretical infrared spectra of compounds **4l** and **5i** are compared in

https://doi.org/10.1021/acsomega.2c06049
ACS Omega 2023, 8, 7415−7429

Table 3. Synthesis of Dihydropyrano[3,2-*c*]chromenes

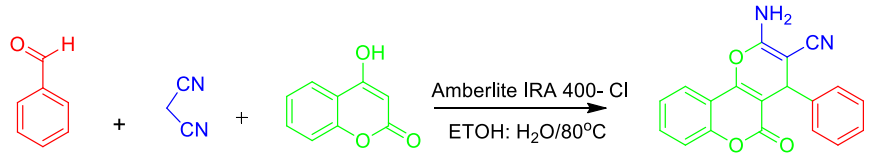

1a-k 2 3b 5a-k

Entry	Aldehyde (1 mM)	Time (hr)	1,3-Diketone	Product/ [yield %]	m. pt.	References °C
1	Benzaldehyde 1a	3	3b	5a [93]	235-240	256-258 [33]
2	4-Nitrobenzaldehyde 1b	3	3b	5b [92]	254-256	256-258[33]
3	4-Cyanobenzaldehyde 1d	3	3b	5c [92]	220-222	225-228[35]
4	2-Chlorobenzaldehyde 1p	3	3b	5d[92]	258-260	262–264[34]
5	4-Fluorobenzaldehyde 1f	3	3b	5e [92]	260-262	262-263[33]
6	2-Hydroxy benzaldehyde 1i	3	3b	5f [92]	245-250	This work
7	Thiophene-2-carboxaldehyde 1j	4	3b	5g [91]	212-214	This work
8	4-Pyridinecarboxaldehyde 1k	4	3b	5h [91]	242-244	This work
9	3-Pyridinecarboxaldehyde 1l	4	3b	5i [92]	250-252	253-259[34]
10	Indole-3-carboxaldehyde 1m	55	3b	5j [90]	198-200	205-206[34]
11	Terephthaldehyde 1n		3b	5k [89]	235-240	This work

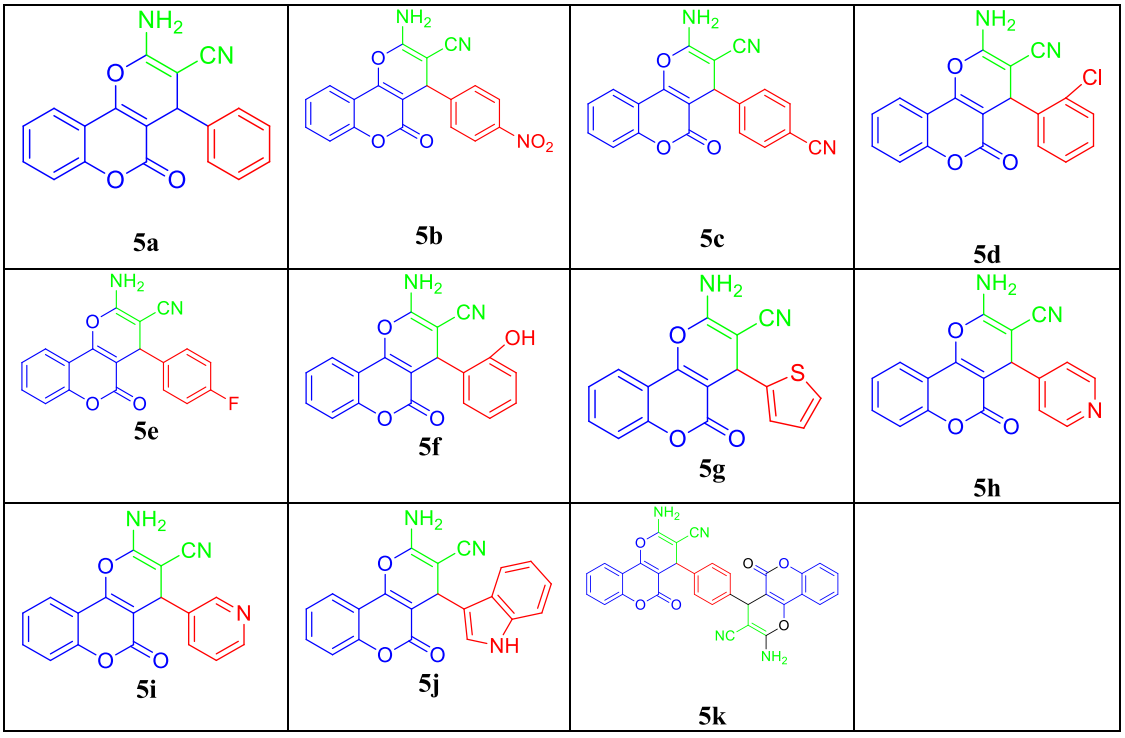

Figure 3. There is a slight deviation in the position of the absorption bands in the experimental and theoretical spectra. In the case of **4l**, the theoretical absorption band for the $-NH_2$ peak was at 3636, and it was at 3633 cm^{-1} for compound **5i**. This almost matches with the experimental values. Theoretical studies show an aromatic −CH stretching vibration at 3226 cm^{-1}, which matches with the 3061 cm^{-1} absorption band determined experimentally. The absorption band for −CN is at

https://doi.org/10.1021/acsomega.2c06049
ACS Omega 2023, 8, 7415−7429

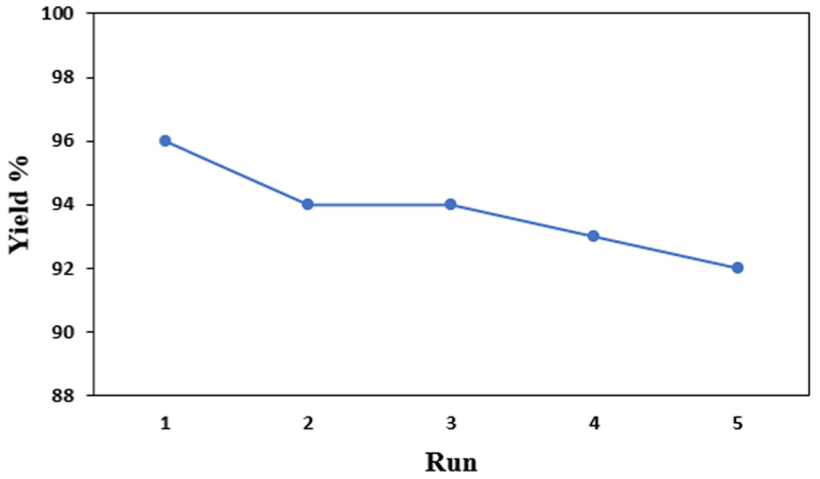

Figure 1. Recyclability of Amberlite IRA-400 (Cl) resin-catalyzed synthesis.

Scheme 1. Plausible Mechanism of the Formation of Chromenes 4 and 5

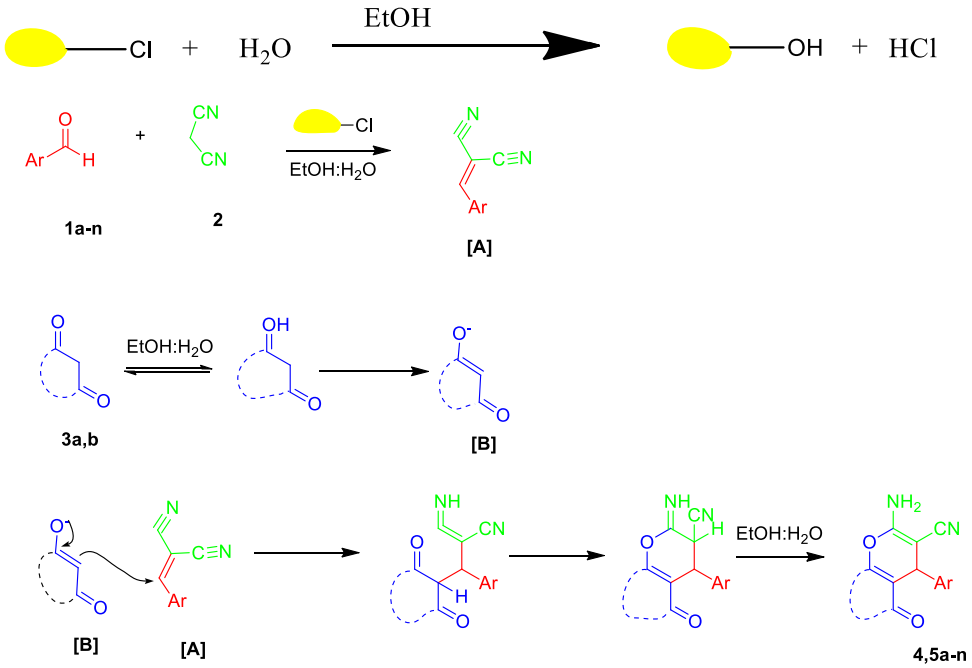

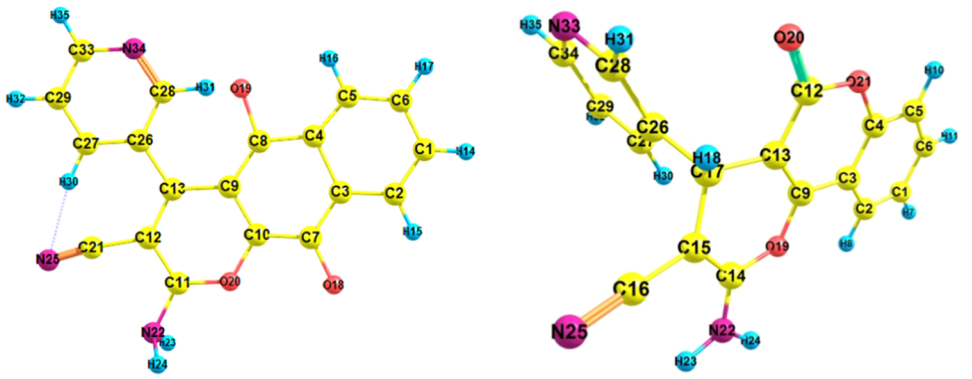

Figure 2. Molecular structures of compounds **4l** and **5i**.

2277 and 2270 cm^{-1} in the theoretical calculation, which is very close to the absorption band at 2198 cm^{-1} obtained experimentally. The C═O absorption band (1757 cm^{-1}) is also in the prescribed range, which also suggests the agreement of the theoretical calculation with the experimental observation.[37]

https://doi.org/10.1021/acsomega.2c06049
ACS Omega 2023, 8, 7415−7429

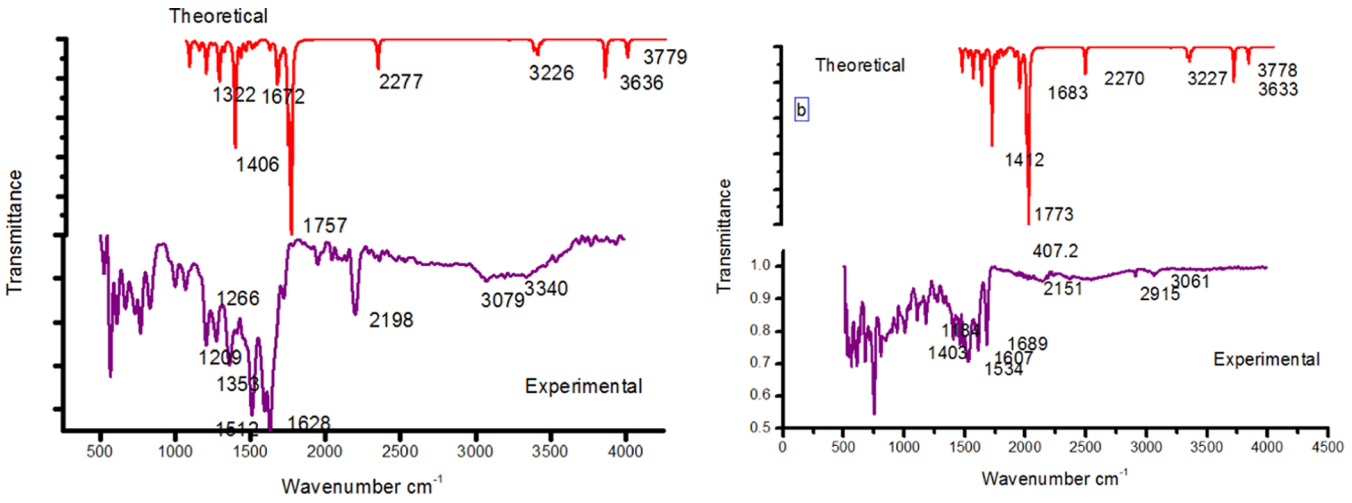

Figure 3. FT-IR spectrum of compounds **4l** and **5i**.

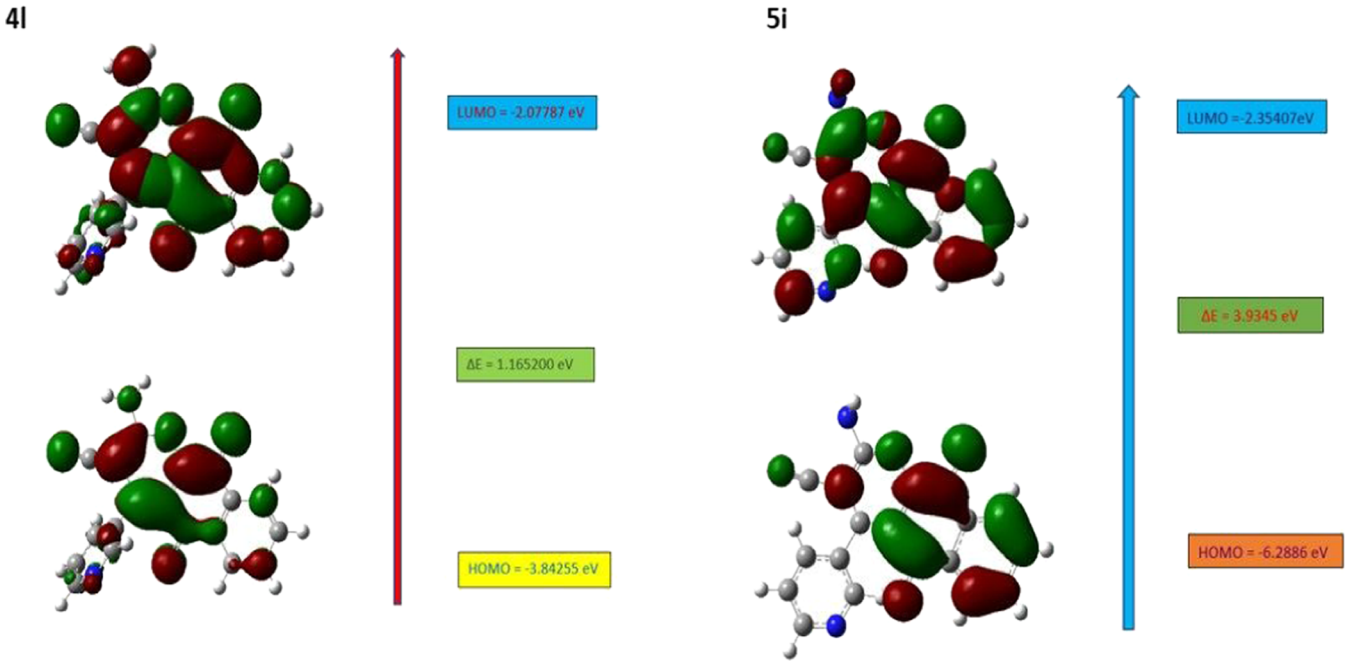

Figure 4. Molecular orbital diagram of compounds **4l** and **5i**.

3.6. FMO Analysis. The frontier molecular orbital analysis provides details on the electron transition from the highest occupied molecular orbital (HOMO) to the lowest unoccupied molecular orbital (LUMO), which are the two types of FMOs. The HOMO represents the ability to donate an electron, the LUMO represents the ability to accept an electron, and the energy difference between the HOMO and LUMO gives the band gap energy; it plays an important role in determining the chemical stability and reactivity of the molecule.[38] The energy level diagram of the compounds is represented in Figure 4. This band gap provides information regarding several global descriptors, which can be calculated from the Koopmans theorem.[37]

3.7. Chemical Reactivity Indices. To obtain a deep understanding of the chemical reactivity of the selected compounds, the global descriptive parameters such as hardness, softness, chemical potential, electronegativity, and electrophilicity index were calculated using Koopmans' theorem as follows: according to the calculation, the energy gap between the orbitals in compound **4l** is 1.165200 eV and that of compound **5i** is slightly higher and is 3.9345 eV.

$$\text{ionization potential (IP)} = -E_{\text{HOMO}} \tag{1}$$

$$\text{electron affinity (EA)} = -E_{\text{LUMO}} \tag{2}$$

$$\text{the hardness } (\eta) = \frac{\text{IP} - \text{EA}}{2} \tag{3}$$

$$\text{the softness, } s = \frac{1}{2\eta} \tag{4}$$

$$\text{the electronegativity } (\chi) = \chi = \frac{\text{IP} + \text{EA}}{2} \tag{5}$$

$$\text{global electrophilicity index } (\omega) = \frac{\mu^2}{2^{\eta}} \tag{6}$$

https://doi.org/10.1021/acsomega.2c06049
ACS Omega 2023, 8, 7415−7429

The calculated global descriptive parameters are given in Table 4.

Table 4. Global Descriptive Parameters

orbital energy	compound **4l**	compound **5i**
E_{Homo}	−3.84255	−6.2886
E_{Lumo}	−2.07787	−2.35407
ΔE	1.165200	3.9345
chemical potential (μ)	−1.76468	−1.96476
chemical hardness (η)	0.88234	1.9672
softness (S)	0.5666	0.2541
electronegativity (χ)	2.96015	4.31885
global electrophilicity index (ω)	1.76439	0.98105

3.8. Molecular Docking Studies. Molecular docking is an essential technique in structure-based drug discovery using computational methods. In a computer-assisted drug design method, pharmacophore-based molecular docking is one of the well-known methods and it helps scientists virtually screen the interaction between the ligand and the target protein and predicts the binding conformations and affinities of any species to the target protein. The molecular docking proceeds through three steps: (i) ligand preparation, (ii) target protein preparation, and (iii) and molecular docking.

3.9. Ligand Preparation. The structures of all the synthesized compounds were drawn using GaussView, and then, their geometries were optimized using the density functional theory (DFT) method with the B3LYP Functional. All geometry optimization calculations were performed using the 6-311G(d,p) basis set, and all calculations were carried out using the Gaussian 09 package. The freely available program Open Babel was used to generate SMILES strings from the representation of the optimized structure and also to get the Protein Data Bank (pdb) format of the ligand.

3.10. Target Protein Preparation. Using the SMILE format of the optimized structure, which is taken as the ligand, various activities of the molecule were predicted using Prediction of Activity of Spectra for Substances (PASS), an online tool. The protein 6i1o, which can be used in the liver fibrosis treatment, was chosen due to its high Pa (probability to be active) value obtained from the Protein Data Bank (www.rcsb.org/pdb/home/home.do). The downloaded protein quality is checked with the Ramachandran plot (Figure 5). From Figure 5, it is clear that the amino acids of the protein are available in the allowed regions of the plot.

3.11. Molecular Docking. To study the molecular mechanism of ligand−protein interactions, Auto Dock suite 4.2.6 software was used. The computation of the atomic charges was done by the Kollman and Gasteiger method after the polar hydrogen was attached. The most popular algorithm Lamarckian genetic algorithm (LGA) available in Autodock was employed for docking. Here, the docking procedure was performed on the two ligands **4l** and **5i** with the protein

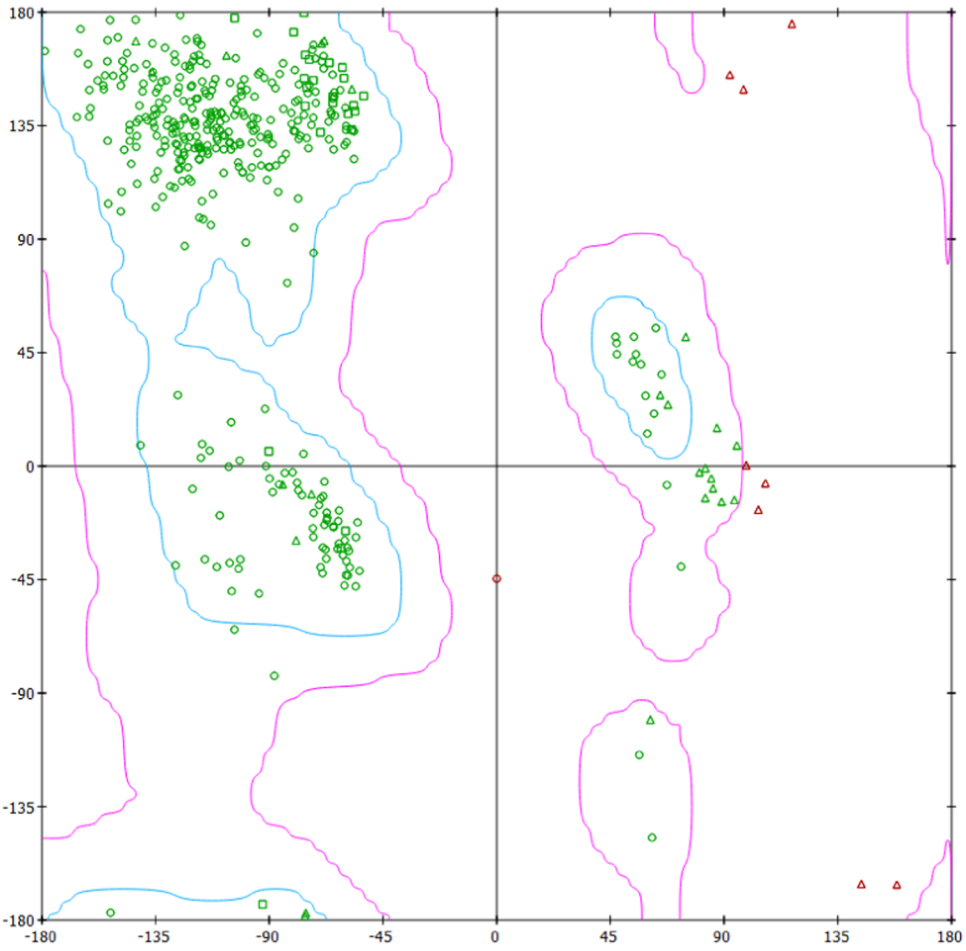

Figure 5. Ramachandran plot of protein 6i1o.

https://doi.org/10.1021/acsomega.2c06049
ACS Omega 2023, 8, 7415−7429

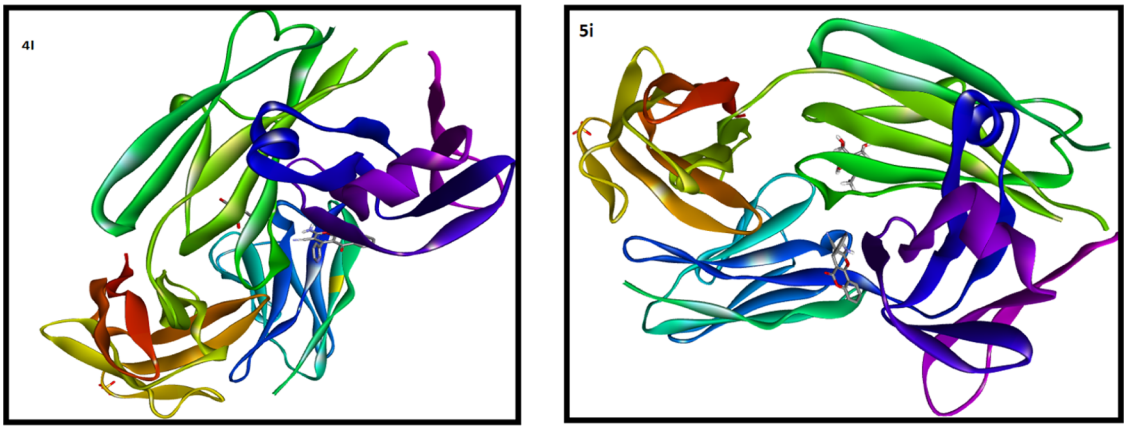

Figure 6. Ligand and the cocrystallized inhibitor embedded into the active site of the 6i1o protein.

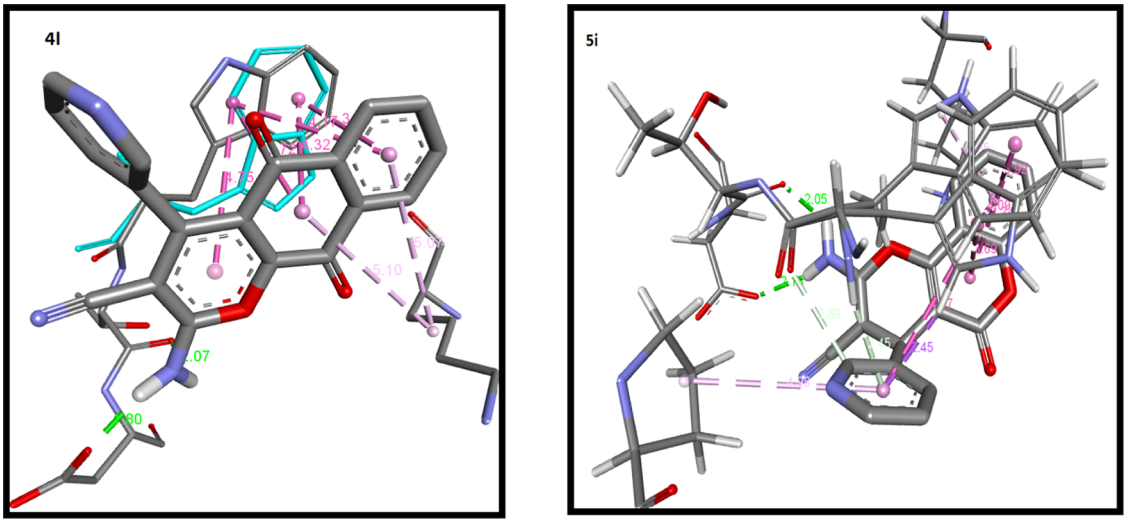

Figure 7. Ligand−protein interactions with their bond distance.

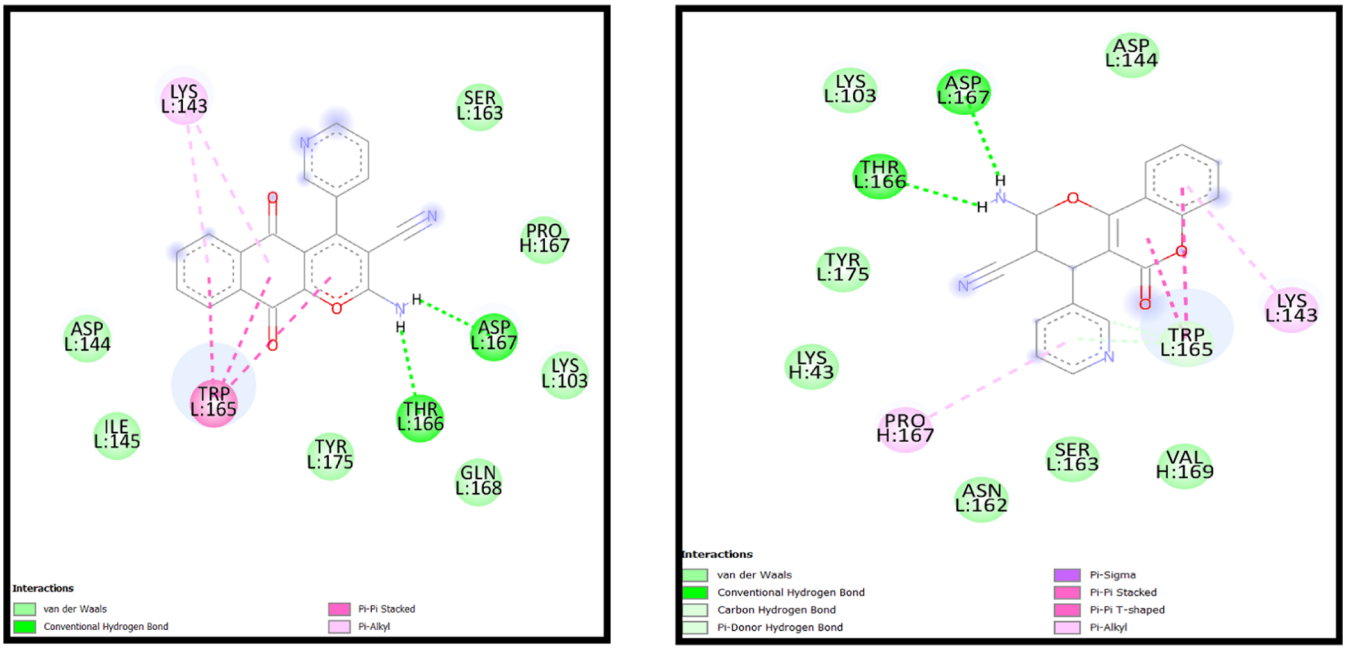

Figure 8. Binding activity of various enzymes of protein 6i1o on the ligands **4l** and **5i**.

https://doi.org/10.1021/acsomega.2c06049
ACS Omega 2023, 8, 7415−7429

prepared. Figure 6 shows the molecular interaction between the ligand and protein along with their binding site.

Figure 7 shows the interaction and the bond distance of the ligand and the cocrystallized inhibitor embedded into the active site of the protein and ligand−protein interactions; H bonds are shown by green dotted lines.

Various enzymes that are bonded to the ligand and the type of bonds formed by them are shown in Figure 8.

Various parameters such s binding energy, bond angle, estimated inhibition constant, and reference root-mean-square deviation (RMSD) were obtained and are listed in Table 5.

Table 5. Docking Parameters of Ligands 4l and 5i

protein (PDB)	estimated inhibition constant (nM)	binding energy (kcal/mol)	intermolecular energy (kcal/mol)	RMSD
4l	41.42	−10.07	−10.64	22.25
5i	43.36	−10.04	−10.67	23.17

The ligand **4l** on interaction with the protein 6i1o exhibits a lower binding energy of −10.07 kcal/mol than that of other ligands **5i**, which shows a binding energy of −10.04 kcal/mol. Also, the inhibition constant of ligand **4l** is 41.42 nM, which is slightly less than that of ligand **5i**, which is obtained as 43.36 nM for the same protein. This suggests the efficiency of the ligand **4l** over other ligands **5i**.

3.12. Anticancer Activity of Dihydropyrano[3, 2-*c*]chromenes and 2-Aminobenzochromenes against Colon Cancer Cells [HT29 Cell Line]. *3.12.1. Chromenes Altered the Cell Morphology and Induced Cell Death in Colon Cancer Cells.* One of the simplest assays to assess cell viability is the MTT assay, which utilizes 3-[4,5-dimethylthiazol-2-yl]-2,5-diphenyltetrazolium bromide (MTT), a yellow dye that produces intense color upon cellular reduction due to the formation of formazan. The principle of the MTT assay depends on the enzymatic conversion of tetrazolium salt MTT into formazan crystals occurring in the mitochondria of living cells. In this study, the cytotoxic effect of the selected compounds has been investigated. The MTT (3-(4,5-dimethyl-thiazol-2-yl)-2,5-diphenyltetrazolium bromide) is a colorimetric assay used for the measurement of cell viability, assessment of cytotoxicity, and determination of cell proliferation.[39,40] Briefly, the MTT is permeable in living cells and also penetrates the mitochondrial membrane. The mitochondria are a vital organelle and contain enzymes to run metabolic processes and importantly the electron transport chain (ETC) for energy production. NAD(P)H-dependent oxidoreductase enzyme plays a key role in MTT assay by reducing the yellow-colored MTT into insoluble purple-colored formazan crystals with the involvement of NADH.[41] The functions of mitochondria are compromised in dead cells due to the depletion of enzymes, and therefore, the reduction of MTT is affected. The purple-colored crystal was dissolved in the DMSO solvent and determined spectrophotometrically. The synthesized compounds were added to HT29 colon cancer cells, and the cell viability was assessed using MTT. From Figure 9, it is clear that the compounds exhibited cell death upon increasing concentrations.

The IC_{50} of the synthesized compounds was determined by MTT Assay. The IC_{50} values of the synthesized compounds **4j**, **4n**, **4m**, **5a**, **5g**, **5j**, and **5k** are 72, 90, 45, 82, 52, 50, and 47 μM, respectively. Cytotoxicity using the compounds (**4j**, **4m**, **4n**, **5a**, **5g**, **5j**, **5k**) was evaluated with standard MTT assays for 12, 24, and 48 h of drug treatment. The plots of cell viability with concentration for the selected compounds are represented in Figure 9. Upon increasing the dose, a significant decline in cells was observed. The data indicate that the proliferation of cancer cells was inhibited in the selected compounds (dihydropyran[3,2-*c*]chromenes and 2-aminobenzochromenes) in a dose-dependent manner, as shown in Figure 10. The MTT data indicate that these compounds altered cell viability.

3.12.2. Dose-Dependent Cytotoxicity of the Selected Compounds. To identify a suitable concentration of the selected compounds capable of inducing a pronounced cytotoxic response in HT29 colon cancer cells, 10, 100, 200, and 300 μM selected compounds were used and evaluated using an MTT-based assay. The dose−response curve of 2-aminobenzochromenes and dihydropyrano[3,2-*c*]chromenes is shown in Figure 10.

3.12.3. Chromene Altered the Cell Morphology in HT29 Cells. The MTT assay revealed the inhibitory effect of compounds in HT29 cells. The morphology of HT29 cells treated with the synthesized compounds was visualized in a light microscope. As shown in Figure 11, the representative image shows morphological changes in control cells (untreated) and treated cancer cells with dihydropyrano[3,2-*c*]chromenes and 2-aminobenzochromenes. Cells were treated with selective compounds for 24 and 48 h. Images were captured in a Motic inverted phase-contrast microscope (Hongkong) at a total magnification of 200×. The compound **4a** treated with HT29 cells exhibited moderate changes compared to the control. The images of **4a** (Figure 11) and **4i** (Figure S44) (both b, c) show the condensed nuclei with cell shrinkage at the initial stage of apoptosis. Similarly, in **4j** cells, cell proliferation was found to be reduced (c) (Figure S44).

Cancer cells at 0 h exhibited abundant growth of cells with well-defined morphology. However, cells treated with chromenes exhibited abundant cell death. The images show a shrinkage in the population of cancer cells (Figures 11 and 12). The images of **4m** (Figure S44) and **4n** (Figure 11) show a shrinkage in the population of cells, indicating their effectiveness in anticancer studies. Images **5j** (Figure S44) and **5k** (Figure 12) also show a shrinkage in the cell population. The images of **5k** at 12 h show that it can almost inhibit the cell population.

The echinoid spikes are increased in images of **5g** (Figure S44) and **4n** (Figure 11). The images of **5k** and **5h** show that most of the cells show shrinkage with a reduced cell size and apoptotic bodies are spotted in **5h** (c). The morphology of **5a** and **5j** shows the changes of phenotypes in most of the cancer cells in the treated group, as depicted in [**5a**(c)], and cell shrinkage with nuclei condensed with membrane blebbing is illustrated in [**5j**(c)].

In this experimental work, the synthesized compounds alter HT29 cancer cells and cause apoptotic features to inhibit cell proliferation. Anticancer compounds kill cancer cells through the induction of apoptosis as an effective mechanism. The accumulating evidence denotes that the apoptotic mode is the preferred one to clear tumor cells. The apoptosis morphology is characterized by condensed nuclei, cell shrinkage, membrane blebbing, apoptotic bodies, and echinoid spikes.[42] These features are in part observed in chromene-treated cells. Condensed nuclei are defined as the breakdown of chromatin

https://doi.org/10.1021/acsomega.2c06049
ACS Omega 2023, 8, 7415−7429

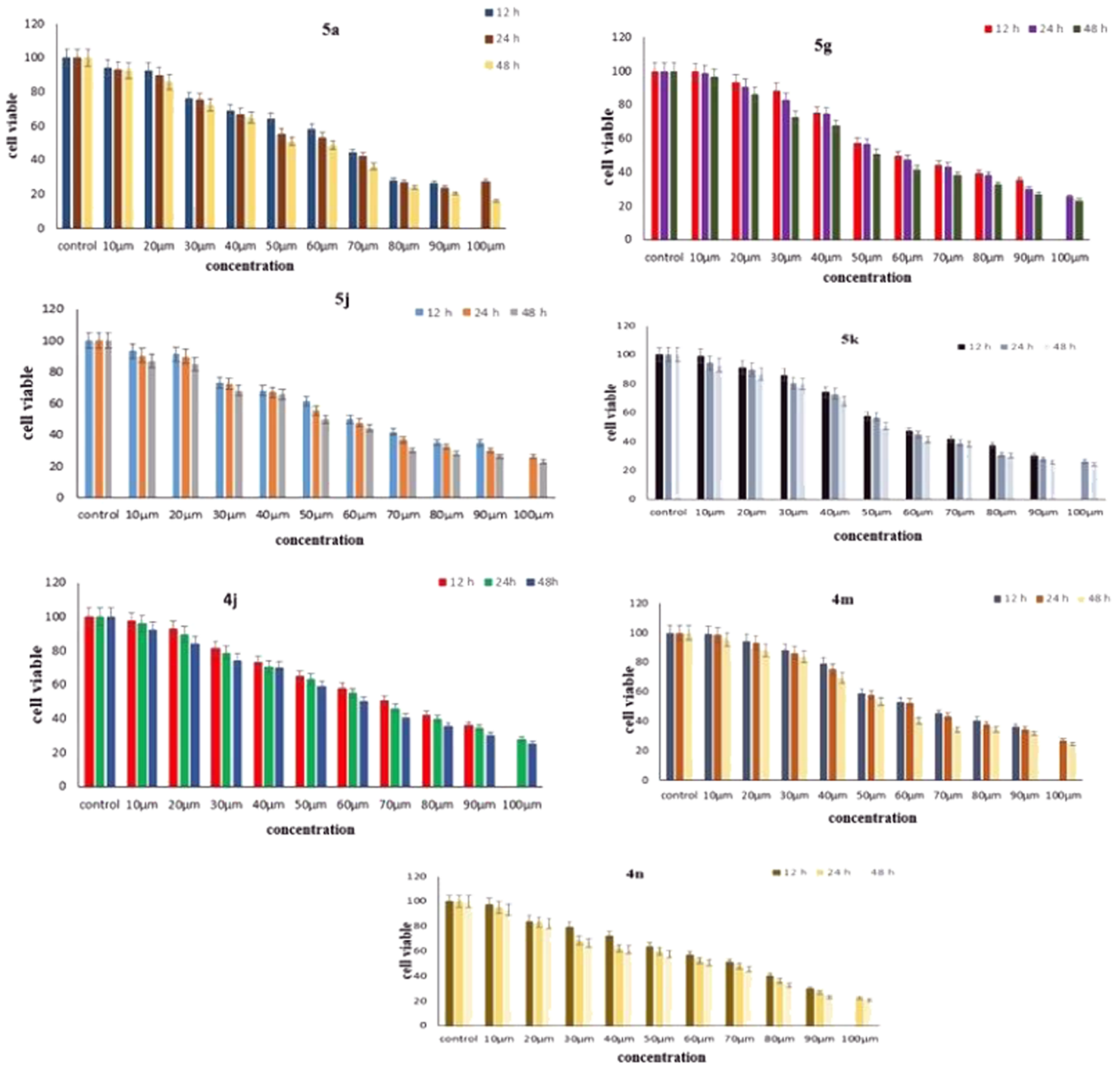

Figure 9. MTT assay of dihydropyrano[3,2-*c*]chromenes and 2-aminobenzochromenes against HT29 colon cancer cells.

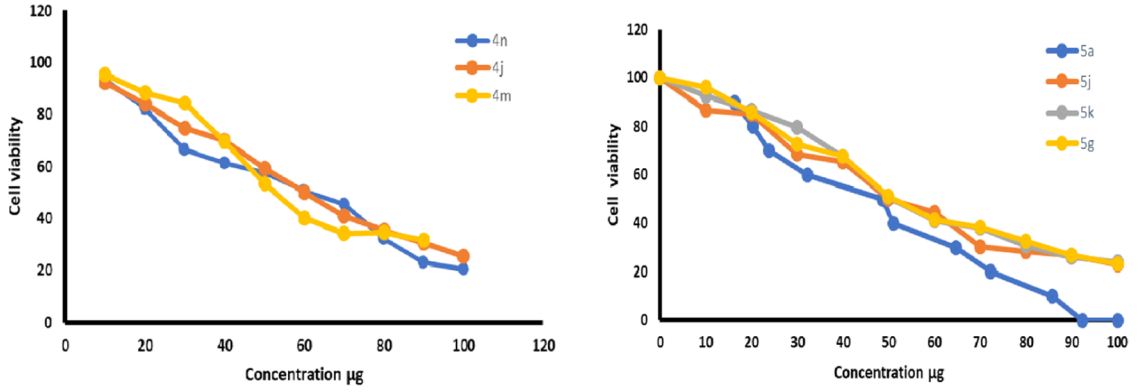

Figure 10. Dose−response curve of (a) 2-aminobenzochromenes (**4j**, **4m**, **4n**) and (b) dihydropyrano[3,2-*c*]chromenes (**5a**, **5g**, **5j**, **5k**) after 48 h.

https://doi.org/10.1021/acsomega.2c06049
ACS Omega 2023, 8, 7415−7429

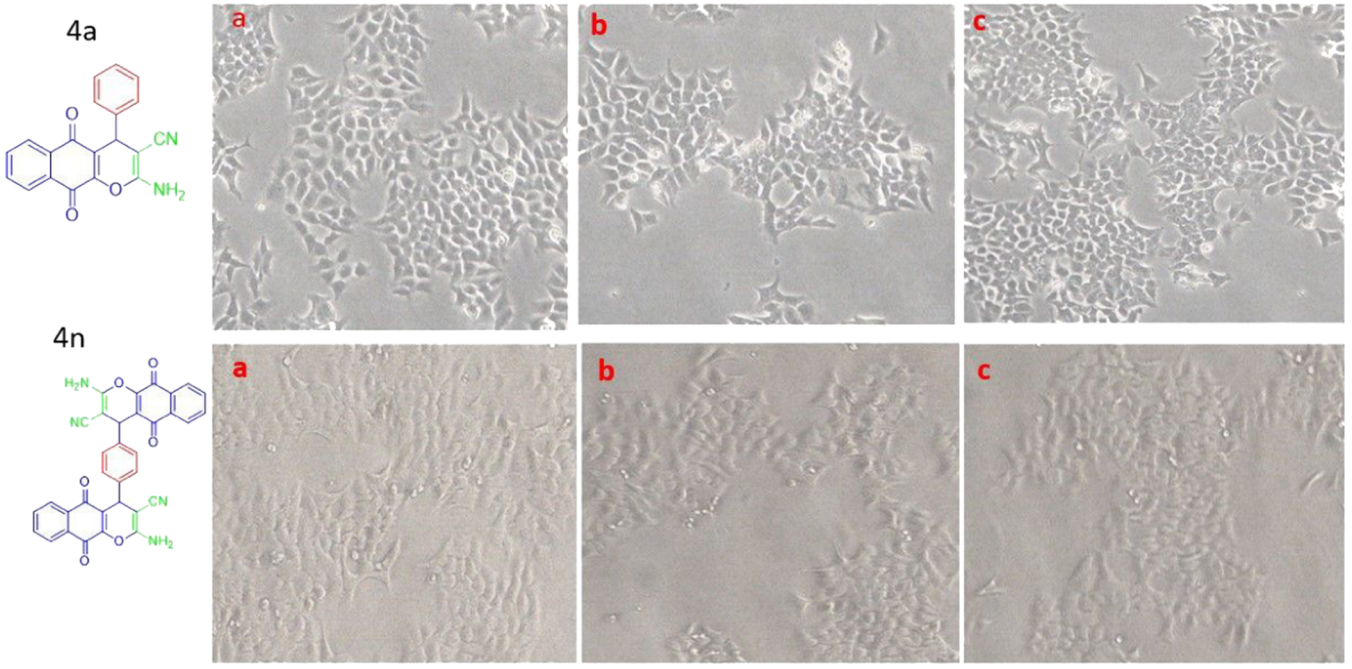

Figure 11. Morphological cell image of 2-aminobenzochromenes after (a) 12 h, (b) 24 h, and (c) 48 h.

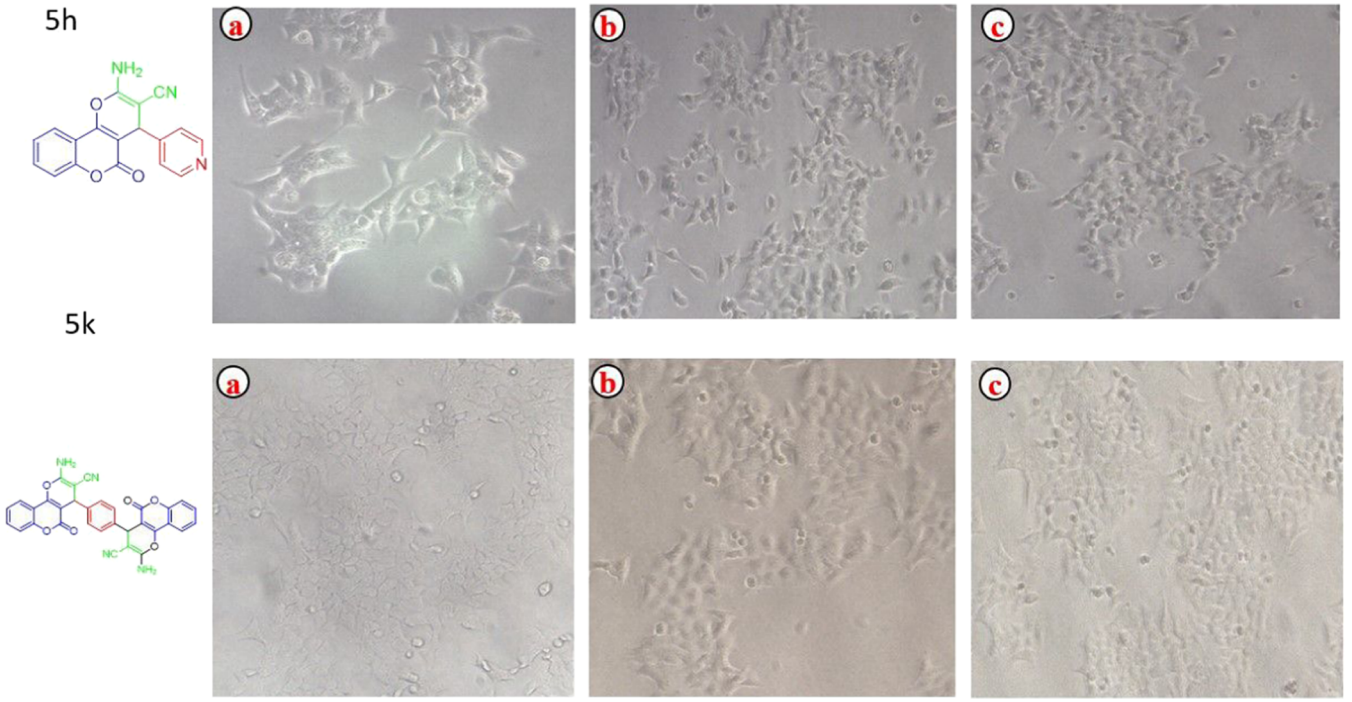

Figure 12. Morphological cell image of dihydropyrano[3,2-*c*]chromenes after (a) 12 h, (b) 24 h, and (c) 48 h.

and with the intact nuclear matrix in the initial stage of apoptosis. Cell shrinkage is the decreased cell size with reduced cell volume in the cytoplasm followed by segregation of the cytoplasm content and nuclear content by packing with the membrane known as membrane blebbing to form apoptotic bodies.[43] Membrane blebbing in the late stage of apoptosis and actually before the formation of apoptotic macrophages can degrade the cells by phagocytosis with their lysosomal enzymes.[44] However, in *in vitro* models, we can visualize the apoptotic body formation with echinoid spikes. Cells undergoing apoptosis lose their cell−cell interaction due to the aberrant expression of cell-adherent molecules and lose cell adhesion characterization from basal attachment. In the treated groups, most of the cells float as compared with control cells. Therefore, the results of MTT and morphology studies revealed that chromene-based synthesized compounds have the potential to inhibit cell proliferation and induce cell death.

3.12.4. DNA Fragmentation Analysis. With the features of apoptosis, the selective synthesized compounds were treated with HT29 cells, and DNA was isolated. Figure 13 shows the nuclear DNA fragmentation as analyzed in agarose gel electrophoresis. Cells undergoing apoptosis exhibit breaks in

https://doi.org/10.1021/acsomega.2c06049
ACS Omega 2023, 8, 7415−7429

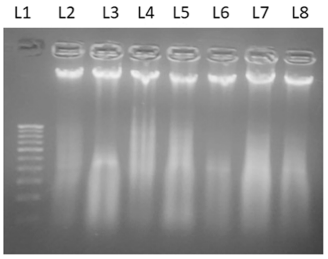

Figure 13. DNA fragmentation analysis by agarose gel electrophoresis. The DNA was isolated from the control and treated groups: L1: DNA ladder, L2: control, L3: **4a**, L4: **4j**, L5: **4k**, L6: **4m**, L7: **4n**, and L8: **5a** are run in 1.5% agarose gel electrophoresis and photographed using an UV transilluminator.

DNA, and therefore, fragmentation was observed as an indication of apoptosis. The normal cells exhibit intact DNA. The synthesized compounds induced DNA fragmentation, which have a lower weight and are easily diffused within the agarose gel.[45] The treated group has high smear, and bands are moving toward the cathode due to the molecular weight being less.

4. CONCLUSIONS

In the end, we would like to conclude this chapter with the following findings:

- We were able to synthesize 2-amino-4*H*-benzo[*g*]-chromene derivatives and dihydropyrano[3,2-*c*]-chromene derivatives via a one-pot multicomponent reaction of 2-hydroxy-1,4-naphthaquinone/4-hydroxy-coumarin, malononitrile, and various aldehydes in the presence of recyclable Amberlite 400-Cl resin as a catalyst.
- The synthesized compounds were characterized and confirmed by necessary spectroscopic methods such as NMR (^{1} H and ^{13} C), FT-IR, and HRMS.
- A plausible mechanism for the formation of 2-amino-4*H*-benzo[*g*]chromenes and dihydropyrano[3,2-*c*]-chromenes was observed.
- The catalyst used for the synthesis had a great advantage, as it was able to recover and be reused for the subsequent reactions.
- Added to the synthesis, one of the synthesized compounds (**4l** and **5i**) was studied theoretically using the DFT method and using the Gaussian 09 package.
- The results obtained from both the theoretical and experimental calculations were compared, and both are in good agreement with each other.
- Molecular docking studies suggest that the ligands **4l** and **5i** are effective against liver fibrosis treatment.
- The anticancer activity of the synthesized compounds against HT29 human colon cancer cells was evaluated through cytotoxicity, morphological analysis, and DNA fragmentation.

■ ASSOCIATED CONTENT

Data Availability Statement

In our study, computational studies were carried out using the Gaussian 09 package, which is available at www.gaussian.com. PDB structures are available from RCSBPDB (https://www.rcsb.org). Molecular docking studies were performed using software AutoDock Tools. (http://autodock.scripps.edu/resources/adt). The ligand and protein molecule preparation was done using PYMOL, which is available at http://pymol.sourceforge.net. The docked structures were viewed in Discovery Studio, which can be obtained from https://discover.3ds.com/discovery-studio-visualizer. The FT-IR spectra were drawn using Origin Lab, which is available at https://www.originlab.com. Produced and analyzed data are available from the authors upon request.

Supporting Information

The Supporting Information is available free of charge at https://pubs.acs.org/doi/10.1021/acsomega.2c06049.

Experimental procedures and compound characterization data (PDF)

■ AUTHOR INFORMATION

Corresponding Author

Harichandran Gurusamy − *Department of Polymer Science, University of Madras, Chennai 600 025, India;* orcid.org/0000-0003-3106-0578; Email: umhari@unom.ac.in, umghari@gmail.com

Authors

Surya Cholayil Palapetta − *Department of Polymer Science, University of Madras, Chennai 600 025, India; Department of Chemistry, Jerusalem College of Engineering, Narayanapuram, Chennai 600 100, India*

Sudhandiran Ganapasam − *Department of Biochemistry, University of Madras, Chennai 600 025, India*

Complete contact information is available at: https://pubs.acs.org/10.1021/acsomega.2c06049

Notes

The authors declare no competing financial interest.

The authors declare that they have no known contending monetary interests or individual connections that might have seemed to impact the work revealed in this paper.

■ ACKNOWLEDGMENTS

The authors thank the University of Madras for providing infrastructure facilities and Director, CSIR-CLRI, for helping with the NMR measurement. S.C.P. thanks the RUSA for providing the project fellowship under RUSA 2.0 (C3/RI&QI/T2/P3/PF1).

■ REFERENCES

(1) Afifi, T. H.; Riyadh, S. M.; Deawaly, A. A.; Naqvi, A. Novel chromenes and benzochromenes bearing arylazo moiety: molecular docking, in-silicoadmet, in-vitro antimicrobial and anticancer screening. *Med. Chem. Res.* **2019**, *28*, 1471−1487.

(2) Ali, K. A.; Abdelhafez, N. A. A.; Ragab, E. A.; Ibrahim, A. A.; Amr, A. E. Design and synthesis of novel fused heterocycles using 4-chromanone as synthon. *Russ. J. Gen. Chem.* **2015**, *85*, 2853−2860.

(3) Sui Xiong, C.; Drewe, J.; Kasibhatla, S. A chemical genetics approach for the discovery of apoptosis inducers: from phenotypic cell based HTS assay and structure- activity relationship studies, to identification of potential anticancer agents and molecular targets. *Curr. Med. Chem.* **2006**, *13*, 2627−2644.

(4) Foroumadi, A.; Emami, S.; Sorkhi, M.; Nakhjiri, M.; Nazarian, Z.; Heydar, S.; Ardestani, S.; Poorraja, F.; Shafiee, A. Chromene-based synthetic chalcones as potent antileishmanial agents: synthesis and biological activity. *Chem. Biol. Drug Des.* **2010**, *75*, 590−596.

(5) Tanaka, J. C. A.; da-Silva, C. C.; Ferreira, I. C. P.; Machado, G. M. C.; Leon, L. L.; de-Oliveira, A. J. B. Antileishmanial activity of

indole alkaloids from Aspidospermaramiflorum. *Phytomedicine* **2007**, *14*, 377−380.
(6) Fadda, A. A.; Berghot, M. A.; Amer, F. A.; Badawy, D. S.; Bayoumy, N. M. Synthesis and antioxidant and antitumor activity of novel pyridine, chromene, thiophene and thiazole derivatives. *Arch. Pharm.* **2012**, *345*, 378−385.
(7) Jain, N.; Jiayi, X.; Ramesh, M. K.; Fuyong, D.; Guo, J. Z.; Emmanuel, P.; et al. Identification and structure-activity relationships of chromene-derived selective estrogen receptor modulators for treatment of postmenopausal symptoms. *J. Med. Chem.* **2009**, *52*, 7544−7569.
(8) Kasibhatla, S.; Gourdeau, H.; Meerovitch, K.; Drewe, J.; Reddy, S.; Qiu, L.; Zhang, H.; Bergeron, F.; Bouffard, D.; Yang, Q.; et al. Discovery and mechanism of action of a novel series of apoptosis inducers with potential vascular targeting activity. *Mol. Cancer Ther.* **2004**, *3*, 1365−1373.
(9) Lee, K. S.; Khil, L. Y.; Chae, S. H.; Kim, D.; Lee, B. H.; Hwang, G. S.; Moon, C. H.; Chang, T. S.; Moon, C. K. (Effects of DK-002, a synthesized (6aS, cis)-9,10- Dimethoxy-7,11b-dihydro-indeno[2,1-c] chromene-3,6a-diol, on platelet activity. *Life Sci.* **2006**, *78*, 1091−109.
(10) Jordão, A. K.; Vargas, M. D.; Pinto, A. C.; de Fernando, C. S.; Ferreira, V. F. Lawsone in Organic Synthesis. *RSC Adv.* **2015**, *5*, 67909−67943.
(11) Sashidhara, K. V.; Kumar, M.; Modukur, R. K.; Srivastava, A.; Puri, A. Discovery and synthesis of novel substituted benzocoumarins as orally active lipid modulating agents. *Bioorg. Med. Chem. Lett.* **2011**, *21*, 6709−6713.
(12) Khurana, J. M.; Nand, B.; Saluja, P. DBU: a highly efficient catalyst for one-pot synthesis of substituted 3,4-dihydropyrano[3,2-c] chromenes, dihydropyrano[4,3-b] pyranes, 2-amino-4Hbenzo[h]-chromenes and 2-amino-4H -benzo[g]chromenes in aqueous medium. *Tetrahedron* **2010**, *66*, 5637−5641.
(13) Daloee, T. S.; Behbahani, F. K. A Green Route for the Synthesis of 2-Amino-5,10-dioxo-4-aryl-5,10-dihydro-4H-benzo[g]chromene-3-carbonitriles using L-Proline as a basic organocatalyst. *Polycyclic Aromat. Compd.* **2022**, *42*, 681−689.
(14) Shaabani, A.; Ghadari, R.; Ghasemi, S.; Pedarpour, M.; Rezayan, A. H.; Sarvary, A.; Ng, S. W. Novel One-Pot Three- and Pseudo-Five Component Reactions: Synthesis of Functionalized Benzo[g]- and Dihydropyrano[2,3-g] chromene Derivatives. *J. Comb. Chem.* **2009**, *11*, 956−959.
(15) Khorami, F.; Shaterian, H. R. Preparation of 2-amino-3-cyano-4-aryl-5,10- dioxo-5,10- dihydro-4H-benzo[g]chromene and hydroxyl naphthalene-1,4-dione derivatives. *Res. Chem. Intermed.* **2015**, *41*, 413171−3191.
(16) Yang, F.; Wang, H.; Jiang, L.; Yue, H.; Zhang, H.; Wang, Z.; Wang, L. A green and one-pot synthesis of benzo[g]chromene derivatives through a multicomponent reaction catalyzed by lipase. *RSC Adv.* **2015**, *5*, 5213−5216.
(17) Akbari, A. One-pot synthesis of dihydropyrano[c]chromene derivatives by using BF3·SiO2 as catalyst. *Heterocycl. Commun.* **2013**, *19*, 425−427.
(18) Farahmand, T.; Hashemian, S.; Shibani, A. ZIF@ZnTiO3 Nanocomposite as Reusable Organocatalyst for the Synthesis of 3, 4-dihydropyrano[c]chromene Derivatives. *Curr. Organocatal.* **2019**, *6*, 256−264.
(19) Mahesh, W.; Pansare, D.; Khan, T.; Pawar, R.; Shelke, R.; Ingle, R. One-Pot Three; Component Synthesis of 2-Amino-5-oxo-4,5-dihydropyrano[3,2-c] chromene-3-carbonitrile Derivatives Catalyzed by Cobalt Doped Iron (III) Tartrate Complex. *Lett. Appl. NanoBioScience* **2022**, *11*, 3208−3217.
(20) Ziarani, G. M.; Badiei, A.; Azizi, M.; Zarabadi, P. Synthesis of 3,4-Dihydropyrano[c]Chromene Derivatives Using Sulfonic Acid Functionalized Silica, (SiO2PrSO3H). *Iran. J. Chem. Chem. Eng.* **2011**, *30*, 59−65.
(21) Mansoor, S. S.; Logaiya, K.; Aswin, K.; NithiyaSudhan, P. Bioactive, An appropriate one pot synthesis of 3,4-dihydropyrano[c]-chromenes and 6-amino-5-cyano-4-aryl-2-methyl- 4H-pyrans with thiourea dioxide as an efficient, reusable organic catalyst in aqueous medium. *J. Taibah Univ. Sci.* **2015**, *9*, 213−226.
(22) Vijender Reddy, A.; Ravinder, K.; Reddy, V. L. N.; Ravikanth, V.; Venkateswarlu, Y. Amberlyst-15 Catalyzed Efficient Synthesis of 1,1-Diacetates from Aldehydes. *Synth. Commun.* **2003**, *33*, 1531.
(23) Pasha, M. A.; Nizam, A. Amberlite IR-120 catalyzed, microwave-assisted rapid synthesis of 2-aryl-benzimidazoles. *J. Saudi Chem. Soc.* **2012**, *16*, 237−240.
(24) Solabannavar, S. B.; Desai, U. V.; Mane, R. B. Heck reaction in aqueous medium using Amberlite IRA-400 (basic). *Green Chem.* **2002**, *4*, 347−348.
(25) Tamaddon, F.; Pouramini, Fl. Amberlyst A26 OH as a Recyclable Catalyst for Hydration of Nitriles and Water-Based Synthesis of 4(1H)-Quinazolinones from 2-Aminobenzonitrile and Carbonyl Compounds. *Synlett* **2014**, *25*, 1127−1131.
(26) Nisar, M.; Ali, I.; Shah, M. R.; Badshah, A.; Qayum, M.; Khan, H.; I Khand, I.; Ali, S. Amberlite IR-120H as a recyclable catalyst for the synthesis of 1,8-dioxo- Octahydroxanthene analogs and their evaluation as potential leishmanicidal agents. *RSC Adv.* **2013**, *3*, 21753−21758.
(27) Taha, M.; Uddin, I.; Gollapalli, M.; Almandil, N. B.; Rahim, F.; Farooq, R. K.; Nawaz, M.; Ibrahim, M.; Alqahtani, M. A.; Bamarouf, Y. A.; Selvaraj, M. Synthesis, anti-leishmanial and molecular docking study of bis-indole derivatives. *BMC Chem.* **2019**, *13*, 102.
(28) Mosmann, T. Rapid colorimetric assay for cellular growth and survival: Application to proliferation and cytotoxicity assays. *J. Immunol. Methods* **1983**, *65*, 55−63.
(29) Brahmachari, G.; Banerjee, B. Facile and one-pot access to diverse and densely functionalized 2-amino-3-cyano-4*H*-pyrans and Pyran-annulated heterocyclic Scaffolds via an eco-friendly multi-component reaction at room temperature using urea as a novel organo-catalyst. *ACS Sustainable Chem. Eng.* **2014**, *2*, 411−422.
(30) Rana, S.; Nagar, A.; Singh, P.; Jain, S. Solvent-free, One pot synthesis of Dihydropyrano [3,2-c] chromene derivatives with *β*-Alanine as a green catalyst. *Eur. J. Mol. Clin. Med.* **2021**, *8*, 1341−1349.
(31) Balalaie, S.; Sheikh-Ahmadi, M.; Bararjanian, M. Tetra-methyl ammonium hydroxide: An efficient and versatile catalyst for the one-pot Synthesis of tetrahydrobenzo[b]pyran derivatives in aqueous media. *Catal. Commun.* **2007**, *8*, 1724−1728.
(32) Frisch, M. J.; Trucks, G. W.; Schlegel, H. B.; Scuseria, G. E.; Robb, M. A.; Cheeseman, J. R.; Scalmani, G.; Barone, V.; Mennucci, 584 B.; Petersson, G. A.; Nakatsuji, H.; Caricato, M.; Li, X.; Hratchian, H. P.; Izmaylov, A. F.; Bloino, J.; Zheng, G.; Sonnenberg, J. L.; Hada, M.; Ehara, M.; Toyota, K.; Fukuda, R.; Hasegawa, J.; Ishida, M.; Nakajima, T.; Honda, Y.; Kitao, O.; Nakai, H.; Vreven, T.; Montgomery, J. A., Jr.; Peralta, J. E.; Ogliaro, F.; Bearpark, M.; Heyd, J. J.; Brothers, E.; Kudin, K. N.; Staroverov, V. N.; Kobayashi, R.; Normand, J.; Raghavachari, K.; Rendell, A.; Burant, J. C.; Iyengar, S. S.; Tomasi, J.; Cossi, M.; Rega, N.; Millam, J. M.; Klene, M.; Knox, J. E.; Cross, J. B.; Bakken, V.; Adamo, C.; Jaramillo, J.; Gomperts, R.; Stratmann, R. E.; Yazyev, O.; Austin, A. J.; Cammi, R.; Pomelli, C.; Ochterski, J. W.; Martin, R. L.; Morokuma, K.; Zakrzewski, V.; Voth, G. A.; Salvador Dannenberg, J. J.; Dapprich, S.; Daniels, A. D.; Farkas, Yazyev.; Austin, A. J.; Cammi, R.; Pomelli, C.; Ochterski, J. W.; Martin, R. L.; Morokuma, K.; Zakrzewski, V. G.; Voth, G. A.; Salvador, P.; Dannenberg, J. J.; Dapprich, S.; Daniels, A. D.; Farkas, Ö.; Foresman, J. B.; Ortiz, J. V.; Cioslowski, J.; Fox, D. J. *Gaussian 09*, revision E.01; Gaussian, Inc.: Wallingford, CT, 2009.
(33) Ben Issa, T.; Ghalla, H.; Marzougui, S. Benhamada, LCrystal structure and theoretical studies on quinoline phosphate. *J. Mol. Struct.* **2017**, *1150*, 127−134.
(34) Ghalla, H.; Issaoui, N.; Govindarajan, M.; Flakus, H. T.; Jamroz, M. H.; Oujia, B. Spectroscopic and molecular structure investigation of 2-furanacrylic acid monomer and dimer using HF and DFT methods. *J. Mol. Struct.* **2014**, *1059*, 132−143.
(35) Kosar, B.; Albayrak, C. Spectroscopic investigations and quantum chemical computational study of (E)-4-methoxy-2-[(p-

https://doi.org/10.1021/acsomega.2c06049
ACS Omega 2023, 8, 7415−7429

tolylimino) methyl] phenol. *Spectrochim. Acta, Part A* **2011**, *78*, 160−167.
(36) Costa, M.; Dias, T. A.; Brito, A.; Proença, F. Biological importance of structurally diversified chromenes. *Eur. J. Med. Chem.* **2016**, *123*, 487−507.
(37) Abd-El-Aziz, A. S.; Alsaggaf, A. T.; Okasha, R. M.; Ahmed, H. E.; Bissessur, R.; Abdelghani, A. A.; Afifi, T. H. Antimicrobial and antitumor screening of fluorescent 5,7-dihydroxy-4-propyl-2h-chromen-2-one derivatives with docking studies. *ChemistrySelect* **2016**, *1*, 5025−5033.
(38) Ghasemi, M.; Turnbull, T.; Sebastian, S.; Kempson, I. The MTT Assay: Utility, Limitations, Pitfalls, and Interpretation in Bulk and Single-Cell Analysis. *Int. J. Mol. Sci.* **2021**, *22*, 12827.
(39) Mosmann, T. Rapid colorimetric assay for cellular growth and survival: application to proliferation and cytotoxicity assays. *J. Immunol. Methods* **1983**, *65*, 55−63.
(40) Freimoser, F. M.; Jakob, C. A.; Aebi, M.; Tuor, U. The MTT [3-(4,5- dimethylthiazol-2-yl)-2,5-diphenyltetrazolium bromide] assay is a fast and reliable method for colorimetric determination of fungal cell densities. *Appl. Environ. Microbiol.* **1999**, *65*, 3727−3729.
(41) Rahman, S. N. S. A.; Wahab, N. A.; Malek, S. N. A. In vitro morphological assessment of apoptosis induced by antiproliferative constituents from the rhizomes of Curcuma zedoaria. *Evidence-Based Complementary Altern. Med.* **2013**, No. 257108.
(42) Toné, S.; Sugimoto, K.; Tanda, K.; Suda, T.; Uehira, K.; Kanouchi, H.; Samejima, K.; Minatogawa, Y.; Earnshaw, W. C. Three distinct stages of apoptotic nuclear condensation revealed by time-lapse imaging, biochemical and electron microscopy analysis of cell-free apoptosis. *Exp. Cell Res.* **2007**, *313*, 3635−3644.
(43) Elmore, S. Apoptosis: a review of programmed cell death. *Toxicol. Pathol.* **2007**, *35*, 495−516.
(44) Arandjelovic, S.; Ravichandran, K. S. Phagocytosis of apoptotic cells in homeostasis. *Nat. Immunol.* **2015**, *16*, 907−917.
(45) Samarghandian, S.; Shabestari, M. M. DNA fragmentation and apoptosis induced by safranal in human prostate cancer cell line. *Indian J. Urol.* **2013**, *29*, 177−183.

https://doi.org/10.1021/acsomega.2c06049
ACS Omega 2023, 8, 7415−7429